Figure S1

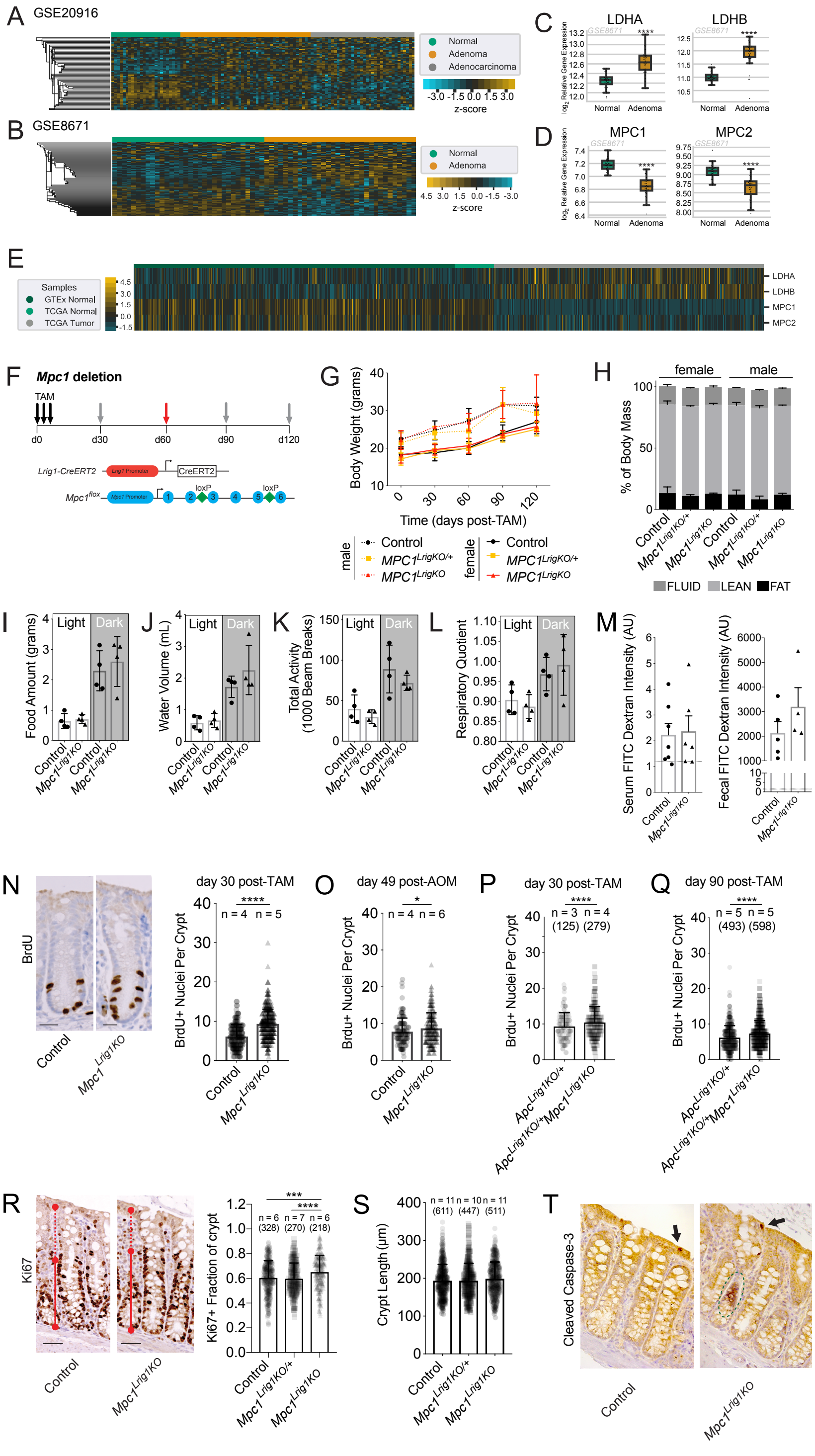
A
GSE20916
Normal
Adenoma
Adenocarcinoma
-3.0 -1.5 0.0 1.5 3.0
z-score
B
GSE8671
Normal
Adenoma
4.5 3.0 1.5 0.0 -1.5 -3.0
z-score
C
LDHA
LDHB
GSE8671
log2 Relative Gene Expression
Normal
Adenoma
D
MPC1
MPC2
E
Samples
GTEx Normal
TCGA Normal
TCGA Tumor
LDHA
LDHB
MPC1
MPC2
F
Mpc1 deletion
TAM
d0
d30
d60
d90
d120
Lrig1-CreERT2
Lrig1 Promoter
CreERT2
Mpc1flox
Mpc1 Promoter
loxP
G
Body Weight (grams)
Time (days post-TAM)
male
Control
MPC1LrigKO/+
MPC1LrigKO
female
H
female
male
% of Body Mass
FLUID
LEAN
FAT
I
Food Amount (grams)
Light
Dark
J
Water Volume (mL)
K
Total Activity (1000 Beam Breaks)
L
Respiratory Quotient
M
Serum FITC Dextran Intensity (AU)
Fecal FITC Dextran Intensity (AU)
N
BrdU
day 30 post-TAM
BrdU+ Nuclei Per Crypt
n = 4 n = 5
O
day 49 post-AOM
Brdu+ Nuclei Per Crypt
n = 4 n = 6
P
day 30 post-TAM
n = 3 n = 4
(125) (279)
Q
day 90 post-TAM
n = 5 n = 5
(493) (598)
R
Ki67
Ki67+ Fraction of crypt
n = 6 n = 7 n = 6
(328) (270) (218)
S
Crypt Length (µm)
n = 11 n = 10 n = 11
(611) (447) (511)
T
Cleaved Caspase-3

Figure S1. Related to Figure 1. Decreased MPC expression enhances crypt basal proliferation without affecting whole animal metabolism.

(A-B) Indicated on the bottom and color bars on the top, GSE20916 (A) and GSE8671 (B) samples were assessed against 80-gene custom probe-set of pyruvate metabolism genes. Probe sets were collapsed as described in the Methods and clustered via calculating the Euclidean distance between centroids. GSE20916 samples were normalized by the original authors using MAS5 and GCRMA with LVS and genes were mean-centered. GSE8671 samples were RMA-normalized using Alt Analyze and genes were mean-centered. (C-D) Normalized $\log_2$ expression levels of *LDHA* and *LDHB* (C), *Mpc1* and *Mpc2* (D) mRNA relative abundance in human colon normal tissue, and adenomas from dataset GSE8671 (n=32), **** FDR<0.0001, error bars SD. (E) Normal colon epithelium gene expression from GTEx (n=339) and TCGA (n=41) compared to TCGA colon adenocarcinomas (n=285) for *MPC1* (FDR=7.71e-95, D=-2.10), *MPC2* (FDR=3.74e-32, D=-0.95), *LDHA* (FDR=1.37e-17, D=0.65), and *LDHB* (FDR=2.86e-27, D=0.92). FDR calculated with Wilcoxon rank-sum test and Cohen's D shows effect size. (F) 8 to 12 week-old transgenic mice were injected intraperitoneally three consecutive days with tamoxifen (TAM;20μg/day), then examined at 30, 60, 90, or 120 days post-TAM. Schematics of the *Mpc1*^{flox} and *Lrig1-CreERT2* alleles are shown. (G) Mouse total body weight was tracked post-TAM (n=10-27 mice per gender), error bars SD. (H) At 60 days post-TAM (*Mpc1* deletion only), body composition of lean, fat and fluid mass relative to total body weight was measured by nuclear magnetic resonance spectroscopy (n=7-10 mice per gender), not significant, one-way ANOVA with multiple comparisons, error bars SEM. (I-L) Mice were placed in Comprehensive Lab Animal Monitoring System Cages for 72 hours, and the last 24 hours of measurements are shown for food intake (I), water intake (J), activity by total beam beaks (K), and respiratory quotient (M) (n=4 males), not significant, unpaired t-test, error bars SD. (L) At 60 days post-TAM, intestinal barrier integrity was assessed by FITC-dextran gavage pulse and six-hour chase with fluorescence assessed in the serum and rectal fecal pellet normalized to PBS-gavaged controls (dotted line) (n=6-7 mice), not significant, unpaired t-test, error bars SD. (N-Q) The number of BrdU-positive nuclei per histologically normal colon crypts in adjacent normal tissue was assessed by immunohistochemistry at 30-days post-TAM (*Mpc1* deletion only) (N) and at 49-days post-AOM (O) in *Mpc1*^{Lrig1KO} and control mice and at 30 (P) and 90 days (Q) post-TAM in *Apc*$^{Lrig1KO/+}$and *Apc*$^{Lrig1KO/+}$*Mpc1*^{Lrig1KO} mice (M; n=4-5 mice, >200 total crypts, N; n=4-6 mice, >100 total crypts, O; n=3-4 mice, >100 total crypts, P; n=5 mice, >300 total crypts), *p≤0.05,**p≤0.01, ****p≤0.0001 by unpaired two-tailed t-test, all error bars SD. (R) Ki67-positive fraction of the crypt was assessed by the portion of crypt length containing adjacent Ki67-labeled nuclei divided by the crypt length

using the line measurement tool on ZEN 2 software at 30 days post-TAM (*Mpc1* deletion only) (n=6-7 mice, >300 total crypts), ***p≤0.001, ****p ≤0.0001, ordinary one-way ANOVA with multiple comparisons, error bars SD. (S) Crypt lengths were assessed using the line measurement tool on ZEN 2 software (n =10-11, >440 total crypts), not significant, ordinary one-way ANOVA with multiple comparisons, error bars SD. (T) The number of cleaved caspase 3-positive nuclei per histologically normal colon crypts in adjacent normal tissue was assessed by immunohistochemistry at 30-days post-TAM in control and *Mpc1*^{Lrig1KO} mice (n=5-7). There were no observed positive nuclei in the crypt and few positive nuclei at the distal luminal surface indicated by the black arrows in representative images (40X, scale bars = 100μm).Green dashed circle shows staining artifact.

Figure S2

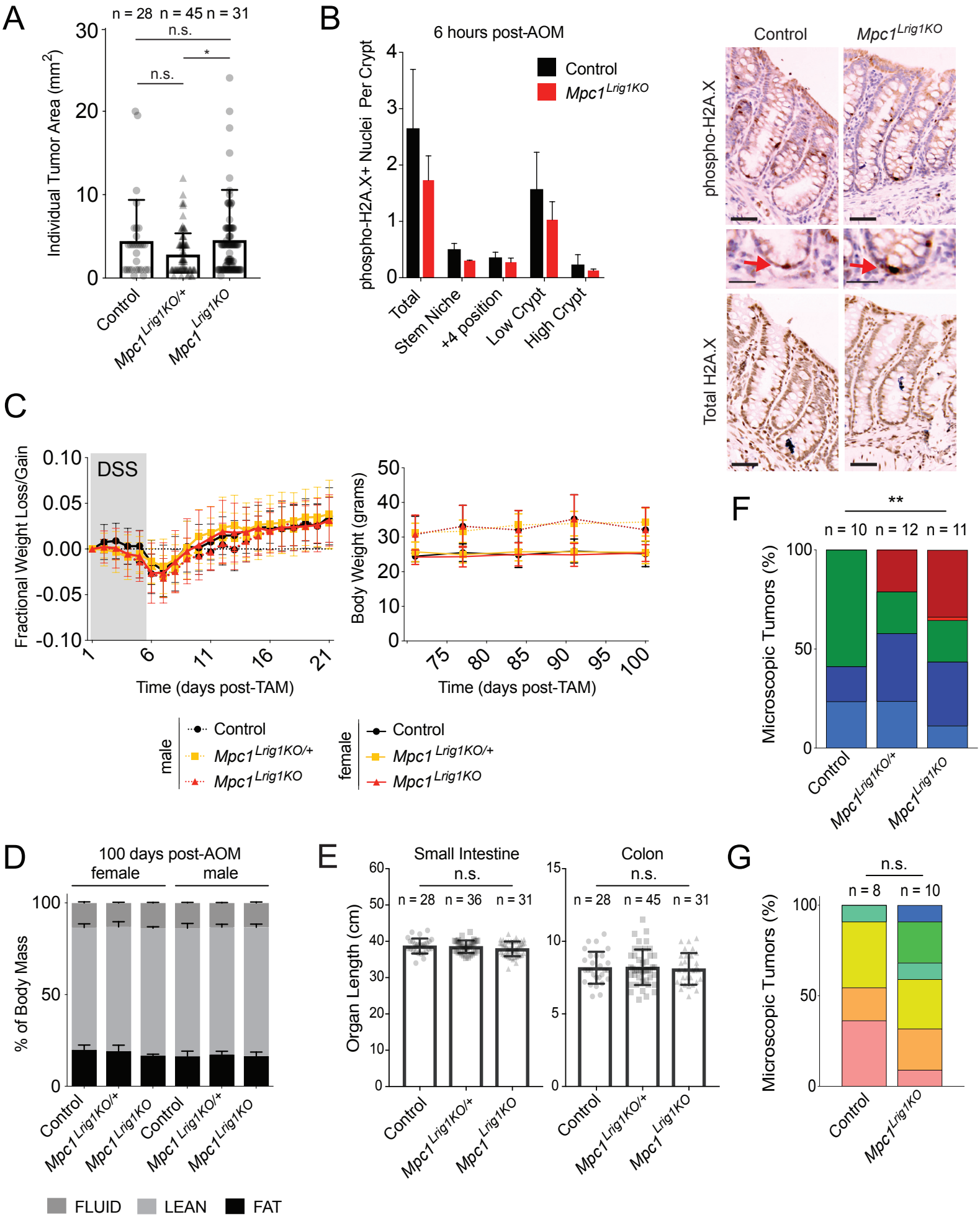
A
n = 28 n = 45 n = 31
n.s.
n.s.
*
Individual Tumor Area (mm2)
Control
Mpc1 Lrig1KO/+
Mpc1 Lrig1KO
B
6 hours post-AOM
Control
Mpc1 Lrig1KO
phospho-H2A.X+ Nuclei Per Crypt
Total
Stem Niche
+4 position
Low Crypt
High Crypt
Control
Mpc1 Lrig1KO
phospho-H2A.X
Total H2A.X
C
DSS
Fractional Weight Loss/Gain
Time (days post-TAM)
Body Weight (grams)
Time (days post-TAM)
male
Control
Mpc1 Lrig1KO/+
Mpc1 Lrig1KO
female
Control
Mpc1 Lrig1KO/+
Mpc1 Lrig1KO
F
**
n = 10 n = 12 n = 11
Microscopic Tumors (%)
Control
Mpc1 Lrig1KO/+
Mpc1 Lrig1KO
D
100 days post-AOM
female
male
% of Body Mass
Control
Mpc1 Lrig1KO/+
Mpc1 Lrig1KO
FLUID
LEAN
FAT
E
Small Intestine
n.s.
n = 28 n = 36 n = 31
Organ Length (cm)
Colon
n.s.
n = 28 n = 45 n = 31
Control
Mpc1 Lrig1KO/+
Mpc1 Lrig1KO
G
n.s.
n = 8 n = 10
Microscopic Tumors (%)
Control
Mpc1 Lrig1KO

Figure S2. Related to Figure 2. Loss of *Mpc1* accelerates tumor initiation and dysplastic progression in the environmental tumor model without enhanced sensitivity to AOM or DSS.

(A) Adenoma size in the colon was assessed by taking two surface measurements of the adenoma's wide and narrow diameters (n=28-45, >30 adenomas), n.s.= not significant, *p≤0.05, one-way ANOVA with multiple comparisons. (B) *Mpc1*^{Lrig1KO} and control mice were injected with azoxymethane (AOM) 6 hours prior to euthanasia. Phospho-H2A.X-positive nuclei were counted and divided by crypt location (n=4 mice, >80 total crypts) as assessed by immunohistochemistry per histologically normal colon crypt (thick scale bars = 20μm, thin scale bars = 10μm). Crypts locations defined as the stem niche (bottom four cells), the +4 position (cell immediately adjacent to the bottom four), the low crypt (lower half of the crypt excluding two previous locations) and the high crypt (upper half of the crypt), not significant, unpaired t-test. (C) Mouse relative weight loss/gain to cycle day 1 body weight was tracked during the three 21-day DSS exposure cycles (left). Mouse total body weight was tracked from 70 to 100 days post-AOM (right). (D) Mouse body composition of lean, fat, and fluid mass relative to total body weight was evaluated at 100 days post-AOM administration by nuclear magnetic resonance spectroscopy (n=7-10 mice/gender), not significant, one way ANOVA with multiple comparisons. (E) At dissection, small intestines were measured from the pyloric sphincter to the ileocecal junction (left) and colons were measured from cecal pouch to the anorectal junction (right) (n=20-54 mice), not significant, one way ANOVA with multiple comparisons. (F) Microscopic tumor grade and size, assessed by pathologic grading in colons of *Mpc1*$^{Lrig1KO/+}$, *Mpc1*$^{Lrig1KO/+}$, and control mice (n=10-12) in Figure 2B was normalized to 100 and analyzed using a Chi-square test on grade only, **p≤0.01. Legend is identical to Figure 2B (Dark Red = High grade >1mm, Red = High grade <1 mm, Dark Green = Focal High Grade >1mm, Light Green = Focal High Grade <1mm, Dark Blue = Low Grade >1 mm and Light Blue = Low Grade <1mm). (G) Regions of superficial inflammation, epithelial injury with active inflammation (AI), aberrant foci, and low-grade dysplasia assessed by pathologic grading in colons of *Mpc1*$^{Lrig1KO/+}$, *Mpc1*$^{Lrig1KO/+}$, and control mice (n=8-10 mice) in Figure 2G, were normalized to 100 and analyzed using a Chi-square test on grade only, n.s.=non-significant. Legend is identical to Figure 2G (Blue = Low Grade, Dark Green = Dysplastic/Inflammatory Focus >1mm, Light Green = Dysplastic/Inflammatory Focus <1mm, Yellow = Surface epithelial injury with active inflammation (AI) >1 mm, Orange = Surface epithelial injury with active inflammation (AI) <1mm, and Pink = Superficial Inflammation.

Figure S3

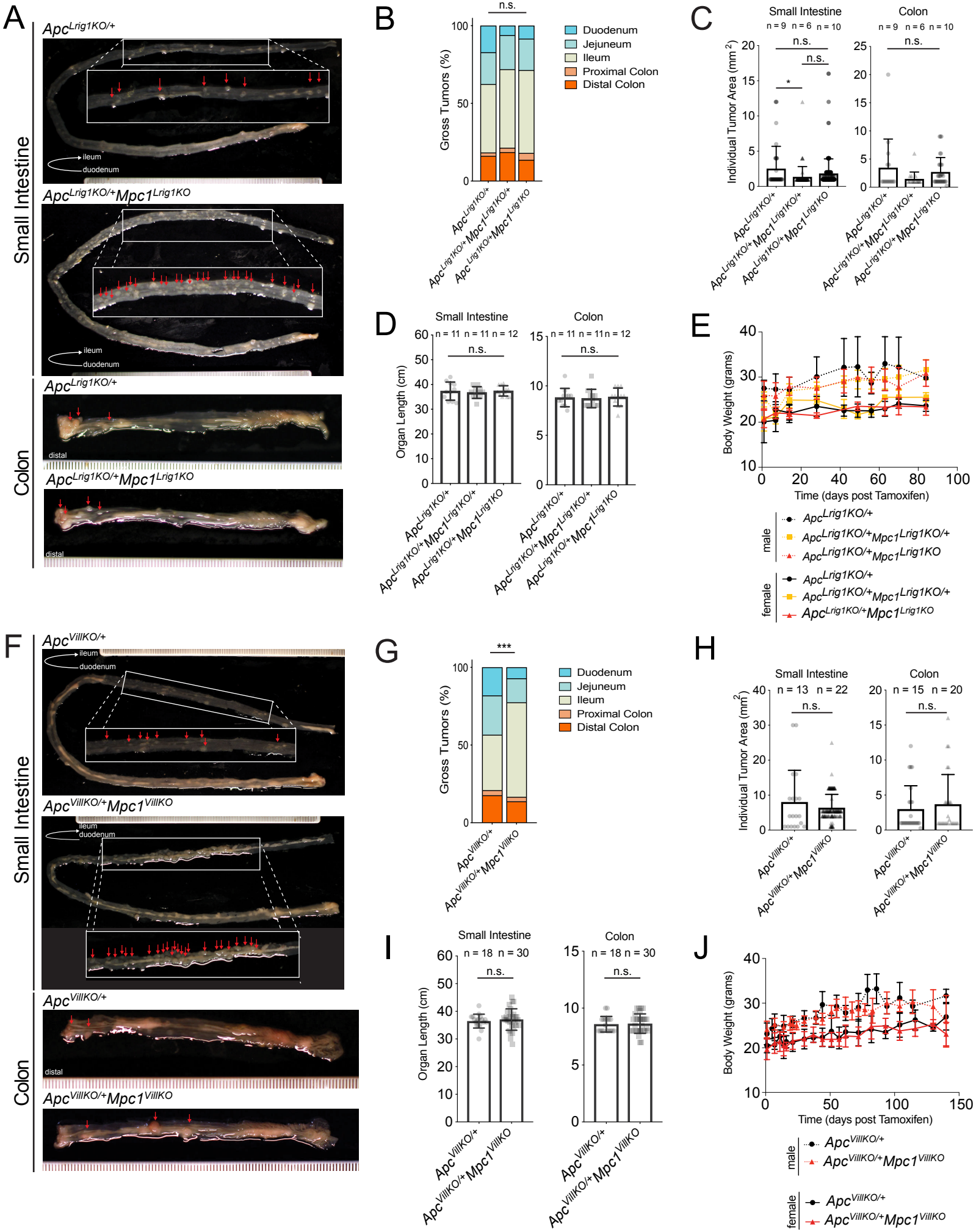
A
Small Intestine
Colon
ApcLrig1KO/+
ApcLrig1KO/+Mpc1Lrig1KO
ileum
duodenum
distal
B
n.s.
Gross Tumors (%)
Duodenum
Jejuneum
Ileum
Proximal Colon
Distal Colon
C
Small Intestine
Colon
n = 9 n = 6 n = 10
n = 9 n = 6 n = 10
n.s.
*
Individual Tumor Area (mm2)
D
Small Intestine
Colon
n = 11 n = 11 n = 12
n = 11 n = 11 n = 12
Organ Length (cm)
E
Body Weight (grams)
Time (days post Tamoxifen)
male
female
F
ApcVillKO/+
ApcVillKO/+Mpc1VillKO
G
***
H
I
n = 18 n = 30
J

Figure S3. Related to Figure 3. *Mpc1* deletion in the small intestine and colon increases dysplastic initiation in the *Apc* loss model of carcinogenesis.

(A) Gross tumor burden of the small intestine (top) and colon (bottom) has individual lesions marked by red arrows (ruler tick = 1mm). (B) Macroscopic tumor distribution across the small intestine and the colon of $Apc^{LrigKO/+}$, $Apc^{LrigKO/+}MPC^{LrigKO/+}$, and $Apc^{LrigKO/+}MPC^{LrigKO}$ mice (n =11-12) was normalized to 100 and analyzed using a Chi-square test, n.s.= not significant. (C) Adenoma size in the small intestine (left) and in the colon (right) was assessed as described in Figure S2A (n=11-12 mice, >15 total adenomas), n.s.=not significant, *p≤0.05, ordinary one-way ANOVA with multiple comparisons. (D) At 90 days post-TAM, small intestines (left) and colons (right) were measured as described in Figure S2E (n=11-12), n.s.=not significant, ordinary one-way ANOVA with multiple comparisons. (E) Following TAM injections, $Apc^{Lrig1KO/+}Mpc1^{Lrig1KO}$, $Apc^{Lrig1KO/+}Mpc1^{Lrig1KO/+}$, $Apc^{Lrig1KO/+}$ mice were tracked for body weight for 90 days. (F) Gross tumor burden in $Apc^{VillKO/+}$ (top) and $Apc^{VillKO/+}Mpc1^{VillKO}$ (bottom) of the small intestine and colon has individual lesions marked by red arrows (ruler tick = 1mm). (G) Macroscopic tumor distribution across the small intestine and the colon of the $Apc^{VillKO/+}Mpc1^{VillKO}$ and $Apc^{VillKO/+}$mice in (n=18-28 mice) in Figure 3G, was normalized to 100 and analyzed using a Chi-square test, ***p≤0.001. (H) Adenoma size in the small intestine (left) and in the colon (right) was assessed as described in Figure S2A (n=18-28 mice, >19 total adenomas), n.s.=not significant, unpaired t-test. (I) At 140 days post-TAM, small intestines (left) and colons (right) were measured as described in Figure S2E (n=18-28 mice), n.s.=not significant, unpaired t-test. (J) $Apc^{VillKO/+}Mpc1^{VillKO}$ and $Apc^{VillKO/+}$ mice were tracked by body weight to 140 days post-TAM.

Supplemental Figure 4

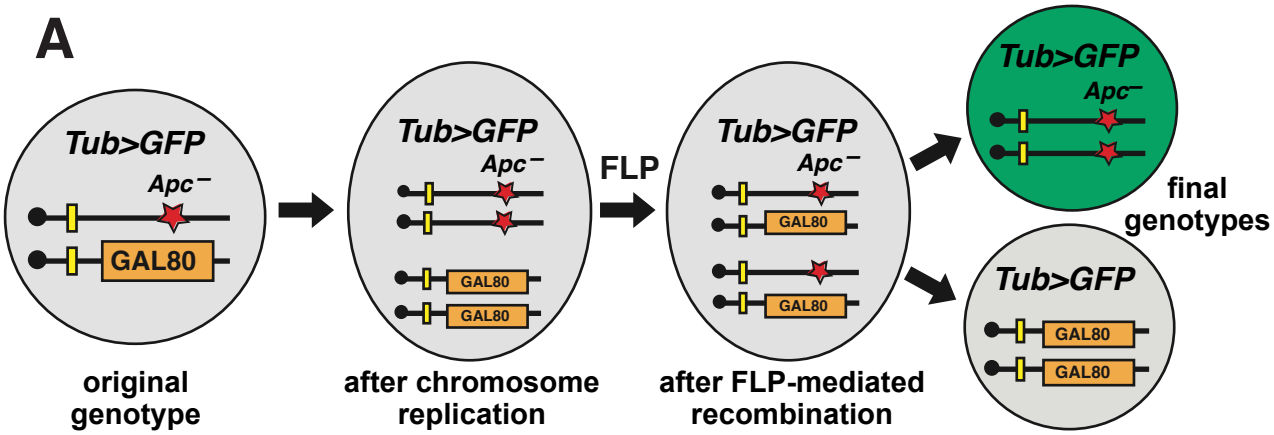

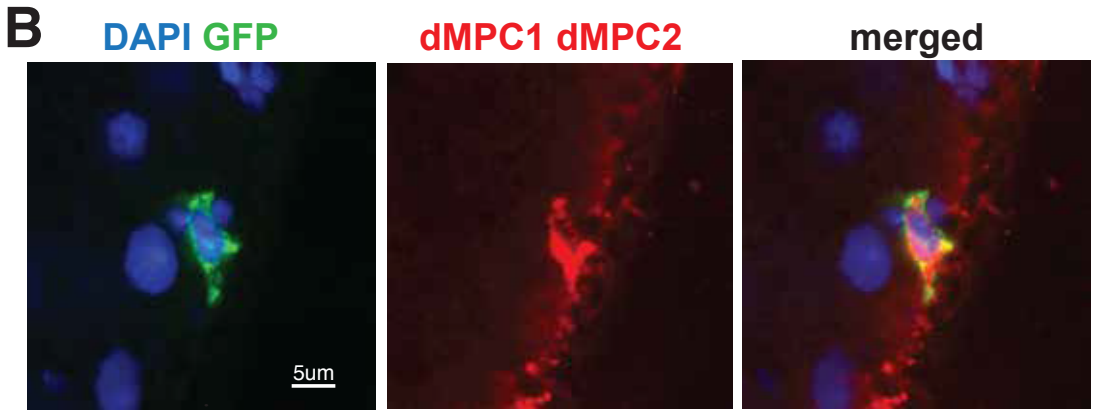

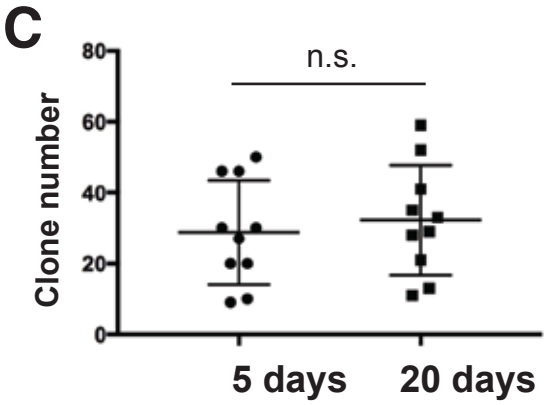

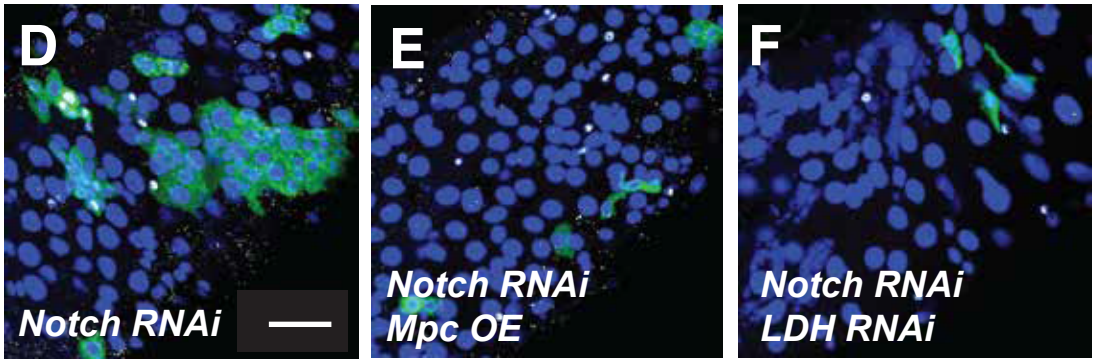

Figure S4. Related to Figure 4 and Figure 5. MPC overexpression arrests oncogenic stem cell expansion

(A) A schematic depiction of MARCM clonal analysis, adapted from Wu and Luo (2006). A *Tub-GAL4* driver is carried in combination with *UAS-GFP* in all cells *(Tub>GFP*). *Tub-GFP* expression is silenced by *Tub-GAL80ts* (GAL80). In the original cell, the chromosome carrying *Tub-GAL80ts* is in combination with a homolog carrying *Apc* mutations (*Apc*$^{-}$). After chromosome replication, Flp-mediated recombination can trigger sporadic recombination at the FRT sites at the base of the homologous chromosomes (yellow boxes). Following mitosis, this will result in one cell that is homozygous for the *Apc1, Apc2* mutations (expressing GFP) and another cell carrying two copies of *Tub-GAL80ts*. If a UAS-driven RNAi transgene (or *UAS-dMPC1-dMPC2*) is included in the genotype, then it will only be expressed in the GFP-labeled *Apc* mutant sister cell and its progeny. (B) Intestinal MARCM clones were generated in *Drosophila* using an *Apc1, Apc2* mutant chromosome with *Tub>dMpc1-dMpc2* overexpression. Clones were analyzed five days after induction using DAPI to stain nuclei (blue) and antibodies to detect either GFP (green) or dMPC1 and dMPC2 protein (red). The row of cells expressing the MPC that lies adjacent to the clone corresponds to visceral muscle. (C) The number of GFP+ clones were counted in intestines from 5 day old and 20 day old flies that carry *Apc1, Apc2* mutations along with MPC overexpression, effectively blocking clonal expansion. No significant difference in clone number was observed between these two time points, n.s.=not signficant, two-tailed Student's t-test). (D-F) Increased mitochondrial pyruvate metabolism blocks Notch enteroendocrine tumor expansion. Intestinal MARCM clones were generated using a chromosome that expresses *Tub> Notch* RNAi either alone (D), or together with *Tub>dMpc1-dMpc2* overexpression (E) or *Tub>LDH RNAi* (F). Immunohistochemistry was performed to detect Prospero, which marks EE cells (small grey nuclei) in intestines for each genotype. No EE cells are detected in clones with MPC overexpression or LDH RNAi. Clones are marked by GFP (green) and nuclei are stained with DAPI (blue).

Figure S5

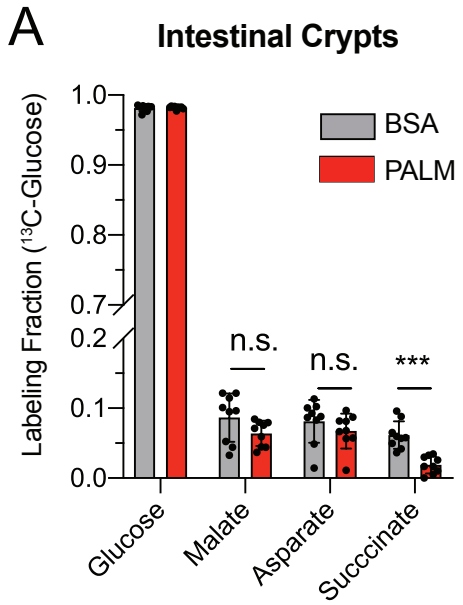
A
Intestinal Crypts
Labeling Fraction (13C-Glucose)
1.0
0.9
0.8
0.7
0.2
0.1
0.0
BSA
PALM
n.s.
n.s.
***
Glucose
Malate
Asparate
Succinate

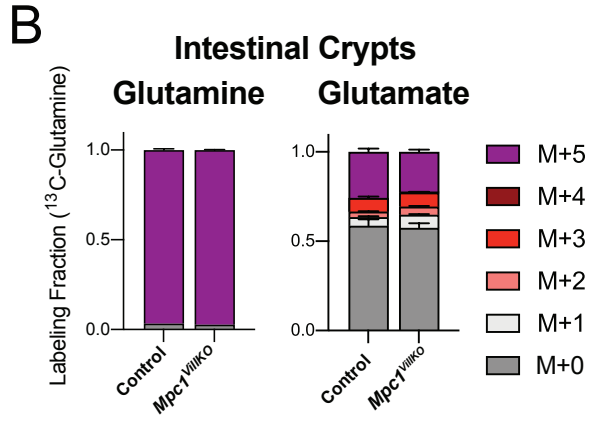
B
Intestinal Crypts
Glutamine
Glutamate
Labeling Fraction (13C-Glutamine)
1.0
0.5
0.0
Control
Mpc1VillKO
M+5
M+4
M+3
M+2
M+1
M+0

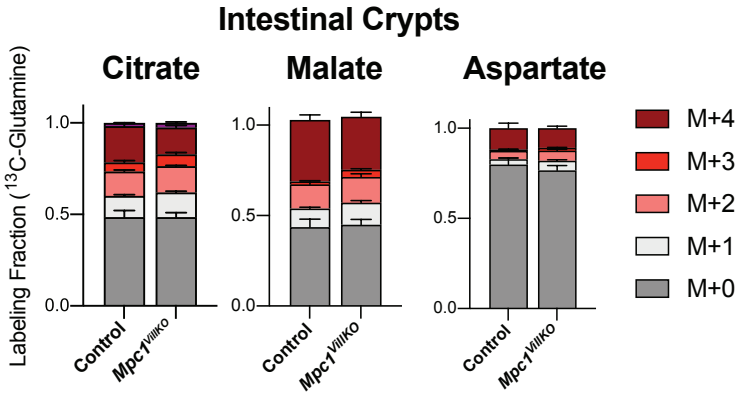
Intestinal Crypts
Citrate
Malate
Aspartate
Labeling Fraction (13C-Glutamine)
1.0
0.5
0.0
Control
Mpc1VillKO
M+4
M+3
M+2
M+1
M+0

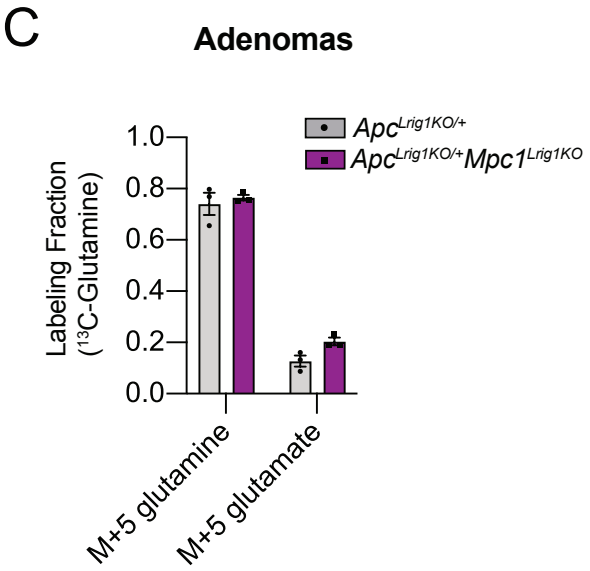
C
Adenomas
Labeling Fraction (13C-Glutamine)
1.0
0.8
0.6
0.4
0.2
0.0
ApcLrig1KO/+
ApcLrig1KO/+Mpc1Lrig1KO
M+5 glutamine
M+5 glutamate

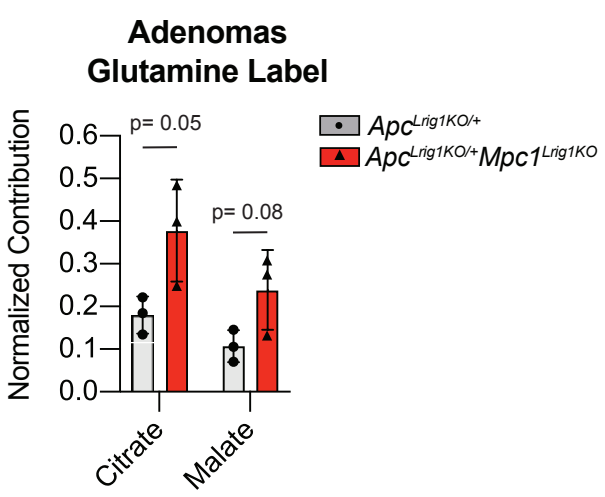
D
Adenomas
Glutamine Label
Normalized Contribution
0.6
0.5
0.4
0.3
0.2
0.1
0.0
p= 0.05
p= 0.08
ApcLrig1KO/+
ApcLrig1KO/+Mpc1Lrig1KO
Citrate
Malate

Figure S5. Related to Figure 6. *Mpc1* loss influences fuel choice in intestinal crypts and adenomas.

(A) The presence of exogenous palmitate in the media does not significantly affect the fractional labeling contribution of glucose to TCA cycle intermediates. Control crypts were incubated with media containing ^{13}C-glucose and either BSA or BSA-palmitate conjugates. In two of the measured TCA cycle compounds, no change in glucose labeling contribution was observed, however in succinate, overall labeling was reduced by around half. For each measured TCA cycle product, labeling was higher without additional palmitate, although it was only significant for succinate. (n=9) ***$p \leq 0.001$, n.s.=not significant, unpaired t-test. (B) ^{13}C-Glutamine and glutamate M+5 labeling is not different between control and *Mpc1*^{VillKO} crypts (left). ^{13}C-glutamine labeling into TCA cycle products citrate, malate and aspartate is not different between control and *Mpc1*^{VillKO} crypts (n=8-9) (right). (C) ^{13}C-Glutamine and glutamate M+5 labeling is not different between *Apc*$^{Lrig1KO/+}$*Mpc1*^{Lrig1KO} and *Apc*$^{Lrig1KO/+}$ adenomas. (D) Normalized contribution of glutamine to citrate and malate production in *Apc*$^{Lrig1KO/+}$*Mpc1*^{Lrig1KO} and *Apc*$^{Lrig1KO/+}$ adenomas. For each metabolite, a normalized labeling fraction was calculated and then corrected for the abundance of the isotopic precursor present in the isolated crypts (n=3 mice, pooled tumors > 3 per mouse) *$p \leq 0.05$, n.s.=not significant, unpaired t-test.

Figure S6

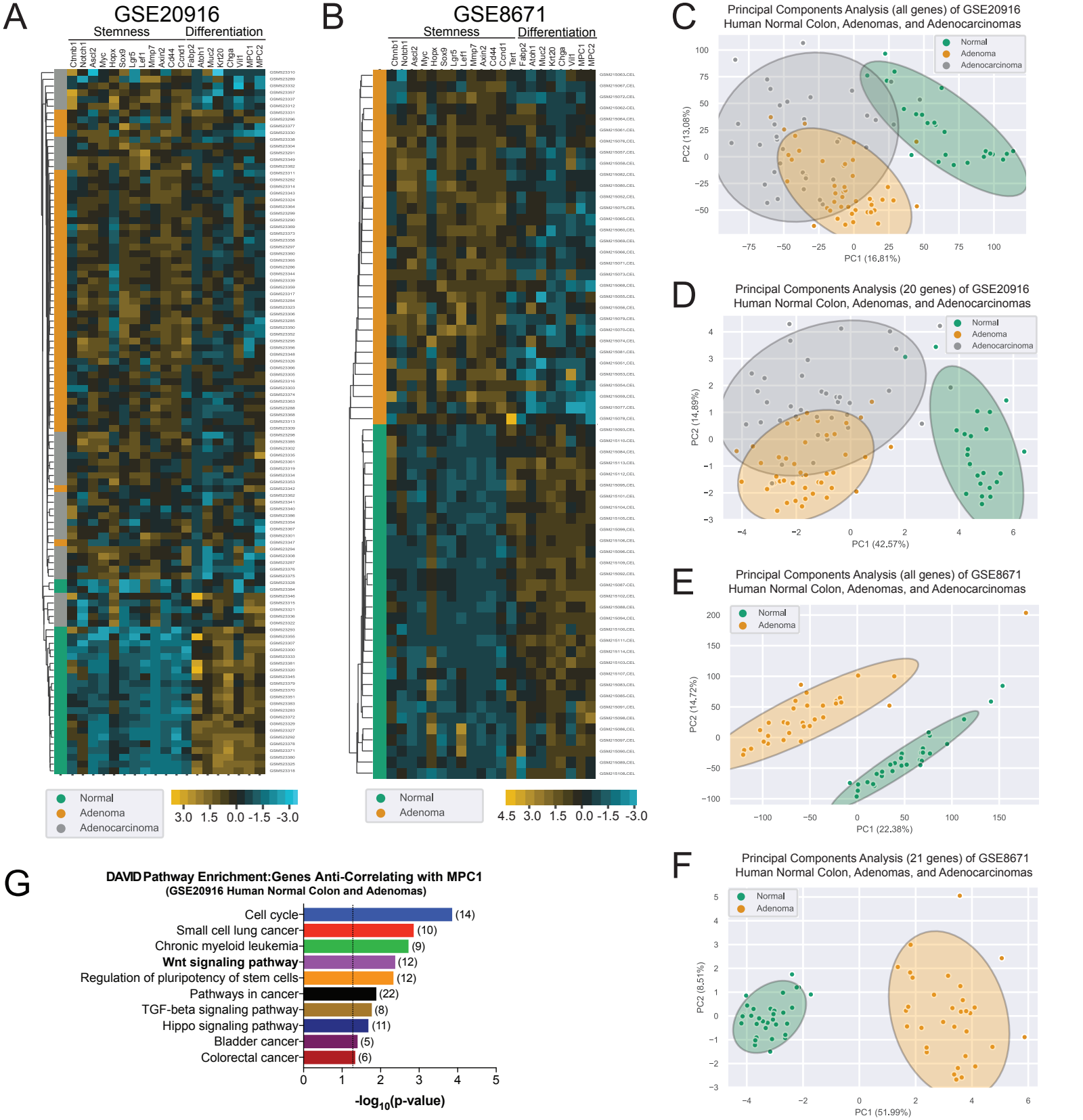
A
GSE20916
Stemness
Differentiation
Ctnnb1 Notch1 Ascl2 Myc Hopx Sox9 Lgr5 Lef1 Mmp7 Axin2 Cd44 Ccnd1 Fabp2 Atoh1 Muc2 Krt20 Chga Vil1 MPC1 MPC2
Normal
Adenoma
Adenocarcinoma
3.0 1.5 0.0 -1.5 -3.0
B
GSE8671
Stemness
Differentiation
Ctnnb1 Notch1 Ascl2 Myc Hopx Sox9 Lgr5 Lef1 Mmp7 Axin2 Cd44 Ccnd1 Tert Fabp2 Atoh1 Muc2 Krt20 Chga Vil1 MPC1 MPC2
Normal
Adenoma
4.5 3.0 1.5 0.0 -1.5 -3.0
C
Principal Components Analysis (all genes) of GSE20916
Human Normal Colon, Adenomas, and Adenocarcinomas
Normal
Adenoma
Adenocarcinoma
PC2 (13.08%)
PC1 (16.81%)
D
Principal Components Analysis (20 genes) of GSE20916
Human Normal Colon, Adenomas, and Adenocarcinomas
Normal
Adenoma
Adenocarcinoma
PC2 (14.89%)
PC1 (42.57%)
E
Principal Components Analysis (all genes) of GSE8671
Human Normal Colon, Adenomas, and Adenocarcinomas
Normal
Adenoma
PC2 (14.72%)
PC1 (22.38%)
F
Principal Components Analysis (21 genes) of GSE8671
Human Normal Colon, Adenomas, and Adenocarcinomas
Normal
Adenoma
PC2 (8.51%)
PC1 (51.99%)
G
DAVID Pathway Enrichment:Genes Anti-Correlating with MPC1
(GSE20916 Human Normal Colon and Adenomas)
Cell cycle (14)
Small cell lung cancer (10)
Chronic myeloid leukemia (9)
Wnt signaling pathway (12)
Regulation of pluripotency of stem cells (12)
Pathways in cancer (22)
TGF-beta signaling pathway (8)
Hippo signaling pathway (11)
Bladder cancer (5)
Colorectal cancer (6)
-log10(p-value)
H
r: -0.73
GSE20916
Normal
Adenoma
Axin2 log2 relative gene expression
Mpc1 log2 relative gene expression
r: -0.67
GSE20916
Normal
Adenoma
Sox9 log2 relative gene expression
Mpc1 log2 relative gene expression
I
r: -0.59
GSE20916
Normal
Adenoma
Adenocarcinoma
Axin2 log2 relative gene expression
Mpc1 log2 relative gene expression
r: -0.61
GSE20916
Normal
Adenoma
Adenocarcinoma
Sox9 log2 relative gene expression
Mpc1 log2 relative gene expression

Figure S6. Related to Figure 7. *Mpc1* anti-correlates with stemness in human adenomas. (A-F) The 20- or 21-gene probe-set included stemness and differentiation marks that separated normal and adenoma tissue shown. GSE20916 (A) and GSE8671 (B) samples were assessed against genes with available probes in the original microarray datasets for the same panel of differentiation/stemness genes as in the mouse models in Figures 4A-B. See Berg 2019 for raw data and analysis code. Probe sets were collapsed as described in the Methods and clustered via calculating the Euclidean distance between centroids. GSE20916 samples were normalized by the original authors using MAS5 and GCRMA with LVS and genes were mean-centered. GSE8671 samples were RMA-normalized using Alt Analyze (See Key Resources Table) and genes were mean-centered. Principle components analysis for all genes (C,E) and 20- or 21-gene paralogs (D,F); *Bmi1* omitted due to multiple mapping probes) for GSE20916 (A,C-D) and GSE8671 (B,E-F), including human normal colon tissue (green), adenomas (orange), and adenocarcinomas (grey, A,C-D only). Ellipses represent the 95% confidence interval and percent variation explained by first and second principle components are reported in the axis labels. (G-I) Linear least squares regression of *Mpc1* gene expression was performed using the adenoma and normal colon samples from GSE201916 and GSE8617. See Berg 2019. (G) GSE20916-derived gene list suggestive of *Mpc1* anti-correlation ($r<-0.6$ and p-value < 0.01) was analyzed by DAVID (v6.8). Negative $\log_{10}$(p-values) are reported for each pathway and the number of genes identified belonging to each pathway is reported to the right of each bar in parentheses. (H) GSE8671-derived joint plots for relative gene expression for *Mpc1* versus Wnt pathway genes *Axin2* (left, p = 3.57E-07) and *Sox9* (right, p = 1.03E-06). The r-value and the fitted regression line with the slope's 95% confidence interval for each correlation are shown. (I) GSE20916-derived joint plots for relative gene expression for *Mpc1* versus Wnt pathway genes *Axin2* (left, p = 2.38E-11) and *Sox9* (right, p = 6.70E-12), including adenocarcinoma. The r-value and the fitted regression line with the slope's 95% confidence interval for each correlation are shown.